JOURNAL OF CATALYSIS 136, 232–241 (1992)

Effect of Alloying on CO Hydrogenation Activity over SiO_2-Supported Co–Ni Alloy Catalysts

TATSUMI ISHIHARA,* NOBUHIKO HORIUCHI, TAKANORI INOUE, KOICHI EGUCHI, YUSAKU TAKITA,* AND HIROMICHI ARAI

*Department of Materials Science and Technology, Graduate School of Engineering Science, Kyushu University, Kasugashi, Fukuoka 816, Japan, and *Department of Environmental Chemistry and Engineering, Faculty of Engineering, Oita University, Oita 870-11, Japan*

Received January 3, 1991; revised November 19, 1991

Alloying Co with Ni is effective for enhancing the activity for CO hydrogenation as well as the selectivity to gasoline. Infrared spectra of adsorbed NO and XPS spectra for the $3p_{3/2}$ orbital of Co and Ni suggest that Co in the alloy interacts electronically with Ni in the outer shell orbital, resulting in the creation of adsorption sites with a new electron density. As a result, alloying Co with Ni strengthens the hydrogen adsorption. Thus alloying Co with Ni allows hydrogen to compete more effectively for adsorption sites in the co-adsorption of CO and H_2. Since the rate of H_2–D_2 exchange on CO preadsorbed Co–Ni alloy shows a good correlation with the CO hydrogenation activity, the reactivity of adsorbed hydrogen in the presence of CO plays a decisive role in determining the activity for CO hydrogenation in this alloy system.

INTRODUCTION

A variety of products with different carbon number is generally obtained in CO hydrogenation over Fischer–Tropsch catalysts. One of the important aims in this reaction is the control of products, in particular, to enhance the selectivity to gasoline. Alloying of metal components has a great effect on the catalytic activity and selectivity because of electronic interaction among the various metal components (*1*). Alloying of metals is expected to be effective in the precise control of selectivity in CO hydrogenation (*2–5*). We have previously reported the high CO hydrogenation activity and high chain growth probability of ternary alloy catalysts of Fe, Co, and Ni (*6–8*). In particular, the Co–Ni alloy is the best candidate for gasoline synthesis among the supported Fe–Co–Ni ternary alloy catalysts.

The co-adsorption behavior of H_2 and CO confirmed that these molecules compete for the same adsorption sites on the metal (*9*). In general, the adsorption of CO is stronger than that of hydrogen (*10, 11*); thus it is well known that the preadsorbed CO species strongly hinder the hydrogen adsorption (*12*). From the theoretical calculation of H and CO coverage on the Ni surface, the adsorption sites were nearly saturated by CO at temperature less than 570 K (*13*). The weakening of CO adsorption, which allows hydrogen to compete more effectively for nickel adsorption sites, leads to higher methanation activity by one or two orders of magnitude (*14*). The adsorption state of hydrogen and carbon monoxide, therefore, has a great significance for determining the catalytic activity and selectivity in CO hydrogenation. In particular, the activation of hydrogen seems to be of primary importance for the CO hydrogenation activity (*15*). However, the reactivity of hydrogen in CO hydrogenation has not been clearly understood up to now partly due to the difficulty of spectroscopic analysis of adsorbed hydrogen. In this study, we investigated the alloy effects on the adsorption states of carbon monoxide and hydrogen on SiO_2-supported Co–Ni alloy catalysts. The H_2–D_2

0021-9517/92 $5.00

exchange reaction was also studied in order to clarify the reactivity of adsorbed hydrogen.

EXPERIMENTAL

The SiO_2-supported Co–Ni alloy catalysts with total metal loading of 10 wt.% were prepared by the incipient wetness technique according to the method described previously (*6*). The catalysts were calcined at 673 K for 4 h and were reduced at 573 K for 2 h and 673 K for 2 h under a hydrogen stream. Catalyst composition is denoted hereafter as *X*Co*Y*Ni, where *X* and *Y* are the atomic percentages of cobalt and nickel, respectively.

Catalytic hydrogenation of carbon monoxide was performed in a high pressure fixed bed flow reactor. The catalyst was preheated in a hydrogen stream at 523 K for 1 h before reaction. A gaseous mixture of H_2(62 vol%), CO(33 vol%), and Ar(5 vol%), which was freed of water and carbonyl impurities by active carbon and 13X-type zeolite, was fed to the catalyst bed at W/F = 10 g-cat h/mol, where W is the catalyst weight and F the total flow rate. The reaction data were taken at 523 K and the total pressure was fixed at 1.0 MPa. The reaction products were analyzed by gas chromatography as reported previously (*6*).

The adsorption state of NO reflects the electron density of the metal (*16*). The infrared spectra of adsorbed NO have been measured to study the electronic state of the alloy. In situ infrared spectra were recorded with a JASCO IR-810 spectrometer. The background spectrum of the catalyst without NO adsorption was subtracted from that with NO adsorption. The electronic state of metal was also studied with XPS. XPS measurements were carried out with a Shimadzu ESCA-850 after reduction at 673 K. Binding energies of Co $3d_{3/2}$ and Ni $3d_{3/2}$ peaks were corrected by comparing the C 1s peak on the sample to that of graphite.

Adsorption rates of H_2 and CO were measured with a conventional volumetric vacuum apparatus. After an evacuation at 673 K, the catalyst was exposed to H_2 and CO. The pressure of CO or H_2 was measured with a Pirani gauge. Desorption rates of H_2 and CO were observed by temperature-programmed desorption (TPD). TPD of hydrogen or carbon monoxide was carried out with a flow system (*6*). The catalyst was reduced in a hydrogen stream at 673 K for 1 h and was evacuated at room temperature for 0.5 h before the TPD measurement of H_2. Carbon monoxide was adsorbed on the prereduced catalysts at 673 K and then was evacuated at room temperature. Argon and helium were used as carrier gases for TPD of H_2 and CO, respectively, after impurity oxygen was removed by electrochemical pumping using yttria-stabilized zirconia as an electrolyte. Desorption of hydrogen or carbon monoxide from the catalyst was monitored by two thermal-conductivity detectors. Water and carbon dioxide were removed with a cold trap which was placed between the detectors.

H_2–D_2 exchange reaction was carried out in a conventional closed circulating system of 120 cm^3 in volume. Gaseous deuterium was obtained by electrolysis of D_2O and commercial hydrogen was purified by passing through a liquid N_2 trap. The mixture with equal amounts of H_2 and D_2 (total pressure is 32.0 kPa) was circulated and the isotope ratio was analyzed by gas chromatography using a $MnCl_2/Al_2O_3$ (10 wt.%) column at liquid N_2 temperature. Before the exchange reaction, the catalyst (0.3 g) was reduced with H_2 at 673 K for 1 h and then evacuated at 673 K for 1 h. The rate of H_2–D_2 exchange, r, was obtained from the following equation (*17*),

$$\log[(X_0 - X_e)/(X_t - X_e)] = rt/2.303N, \quad (1)$$

where t stands for the reaction time, N the total molar amount of hydrogen isotopes (H_2 + D_2 + HD) in the system, and X_0, X_t, and X_e are the molar fraction of HD at 0 sec, t sec, and in equilibrium, respectively.

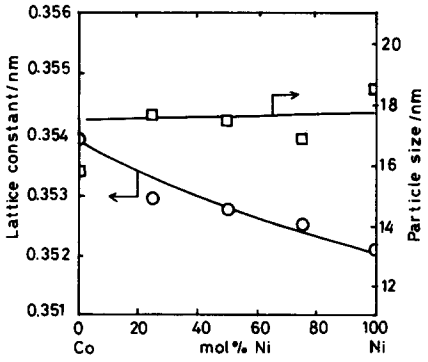

FIG. 1. Lattice constant and particle size of SiO_2-supported Co-Ni alloy as a function of alloy composition: (○) Lattice constant, (□) particle size.

RESULTS AND DISCUSSION

Lattice Constant and Crystallite Size of Supported Co–Ni Alloy

X-ray diffraction was performed after reduction at 673 K to determine the crystallite size and the lattice constant of the alloy catalysts. Only the diffraction peaks from the fcc-structured Co, Ni, and bulk alloy were detected except for peaks from the SiO_2 support (*18*). The crystal structure of Co was transformed from hcp to fcc around 700 K. Catalysts were reduced at 673 K in this study, and so fcc-structured Co was prepared in this study. The lattice constant of Co–Ni alloy obtained from the strongest diffraction peak from the (111) plane is shown in Fig. 1 as a function of alloy composition. The lattice constant of the Co–Ni alloy slightly decreases with increasing Ni content. This suggests that the Co–Ni ordered alloy with fcc structure is formed in each of the SiO_2-supported Co–Ni alloy catalysts. The average crystallite size of the supported metal was estimated with the Scherrer equation from the line broadening of diffraction peak (Fig. 1). Although a slight deviation was recognized, the average crystallite size of the alloy can be regarded as almost the same among the catalysts. Part of the catalyst was subjected to measurement of the metal particle size distribution with a TEM observation. Metal particle sizes ranged from 3 to 20 nm with an average of about 15 nm, which is in fair agreement with that obtained from XRD.

Catalytic Activity and Selectivity for CO Hydrogenation

Catalytic activity and selectivity for CO hydrogenation on SiO_2-supported Co–Ni alloy are shown in Fig. 2 as a function of Ni content. In Fig. 2, hydrocarbon products are grouped into four categories according to their carbon number, i.e., methane, C_2–C_4 olefins, C_2–C_4 paraffins, and C_{5+} hydrocarbons with five or more carbon atoms, which mainly consisted of gasoline compounds. In some cases, a small amount of oxygenated compounds such as alcohol and ester was produced, but no carbon dioxide was produced on any catalyst (*6*). Alloying Co with Ni enhanced the catalytic activity for CO hydrogenation. Among the Co–Ni alloy catalysts, 50Co50Ni shows the highest CO conversion, which is almost six times higher than that of Co and Ni single metal. The Co–Ni alloy catalysts showed a high selectivity to higher hydrocarbons, in particular, to gasoline compounds, but are unselective for methanation. Alloying Co with Ni, therefore, increased not only the CO

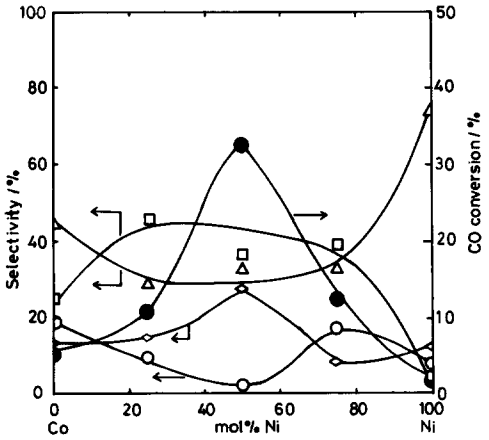

FIG. 2. Catalytic activity and selectivity in CO hydrogenation over SiO_2-supported Co-Ni alloy catalysts as a function of Ni content: (●) CO conversion, (△) CH_4, (○) C_2–C_4 olefins, (◇) C_2^-–C_4^- paraffins, (□) C_{5+}.

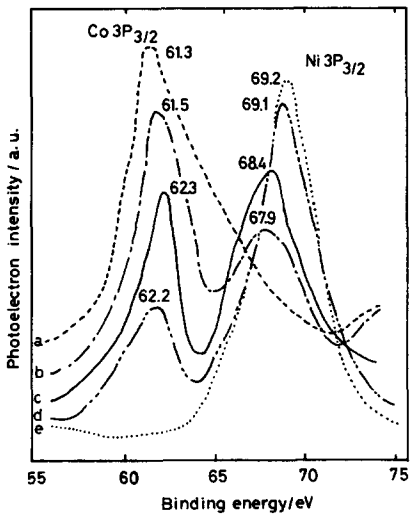

FIG. 3. XPS spectra for the $3p_{3/2}$ orbital of Co and Ni in Co–Ni alloy catalysts: (a) Co, (b) 75Co25Ni, (c) 50Co50Ni, (d) 25Co75Ni (e) Ni.

conversion but also the selectivity to gasoline. The yield of gasoline attained on 50Co50Ni was as high as 15%. Comparing with the yield of other Fischer–Tropsch catalysts, this yield was classified into the highest group at the reaction condition examined. Therefore, Co–Ni alloy catalyst at the equimolar composition is one of the best candidates for the gasoline synthesis from CO hydrogenation, as already reported (*6, 7*).

Electronic State of Adsorption Sites on Co–Ni Alloy Catalyst

Effects of alloying on catalysis are generally classified into two groups; electronic (*1, 19, 20*) and geometric effects (*21–24*). It is reported that the geometric effect is dominant on Cu–Ni alloy catalyst (*25*). An electronic ligand effect, however, is anticipated on alloy consisting of group VIII metals themselves because of the similarity in the electronic configurations (*19, 26*).

XPS spectra for the $3p_{3/2}$ orbital of Co and Ni in alloy catalyst are shown in Fig. 3. The $3p_{3/2}$ orbital is the highest occupied orbital of these metals. The binding energy for the $3p_{3/2}$ electron of Co increased, but that of Ni decreased. Furthermore, the binding energy for the $3p_{3/2}$ electrons of Co and Ni increased with increasing Ni content in alloy. On the other hand, an energy shift could not be recognized on the binding energy of the $2p_{3/2}$ electrons of Co and Ni in the alloy. Thus, the electronic configuration of Co and Ni seems not to be affected significantly by alloying as suggested by a band structure calculation (*27, 28*). However, the higher and lower shifts in the $3p_{3/2}$ peaks of Co and Ni, respectively, suggest that Co in the alloy interacts electronically with Ni at the $3p$ level, and it is expected that a part of the electronic charge in the outer shell of Co is donated to Ni, or an intra-atomic reorganization of the valence electrons of Co and Ni is produced by alloying (*28*). Electronic interaction at the outer shell orbital was also pointed out in the other kinds of alloy systems (*29, 30*). It is expected that the effects of the electron transfer would be restricted to the outer shell orbital. This is because electrons in the inner shell orbital are more strongly attracted by nuclear (screen) effects and the changes in the electronic states by alloying are very small due to the large number of the valence electrons. Since the electron in the outer shell orbital is used when a gaseous molecule adsorbs on the metal, alloying Co with Ni could bring about a marked change in the adsorption property because of the electronic interaction between Co and Ni in the outer shell orbital.

The effect of electronic interaction between Co and Ni on the adsorption behavior of the alloy can be further investigated using the infrared spectra of adsorbed NO as a probe. We have reported previously that the infrared spectra of adsorbed NO are sensitive enough to study the electronic state of surface adsorption sites (*31*). Two infrared bands around 1800 and 1860 cm^{-1} generally appeared on Co–Ni alloy catalysts. The absorption band at 1860 cm^{-1} was still present even after evacuation at 573 K, but that of 1800 cm^{-1} almost disappeared. Two types of adsorbed NO, i.e., bent-type and linear-

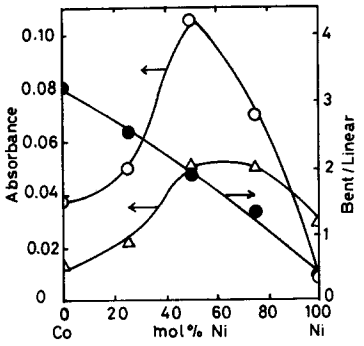

FIG. 4. Dependence of the absorbance of linear- and bent-type NO and its ratio on the alloy composition: (○) Bent-type NO, (△) linear-type NO, (●) ratio of the absorbance of bent- to linear-type band.

type, have been observed so far by IR measurement at 1720–1520 and 1900–1700 cm^{-1}, respectively (*16*). Since the bonding of N–O in bent-type NO is weaker than that in linear-type NO and its stretching band appears at lower wavenumber, the absorption bands at 1860 and 1800 cm^{-1} can be assigned to linear-type and bent-type NO, respectively. Bent-type is formed by electron donation from the metal to the antibonding orbital of the NO molecule, but linear-type is formed by electron withdrawal from NO. The absorbance of bent- and linear-type NO seems to reflect the number of electron-donating and electron-withdrawing sites, respectively, by assuming that an extinction coefficient of bent- and linear-type NO is independent of the alloy composition. The ratio of the absorbance of bent- to linear-type NO, therefore, qualitatively reflects the electron-donating properties of the surface adsorption sites on the alloy. The absorbance of linear- and bent-type NO and its ratio are plotted versus the alloy composition in Fig. 4. Linear-type NO adsorption is dominant on Ni/SiO_2, but the absorbance of bent-type band is strong on Co/SiO_2. This suggests that Co/SiO_2 and Ni/SiO_2 exhibit the electron-donating and electron-accepting property, respectively. The work functions of Co and Ni are 5.00 and 5.14 eV, respectively (*32*). The electron affinity of Ni is stronger than that of Co considering from the work functions. Therefore, the adsorption states of NO on Co and Ni are in good accord with the expectations based on the work functions. On the other hand, the ratio of these two absorption bands linearly decreased with increasing Ni content. It is expected that the electronic state of surface adsorption sites altered linearly from Co to Ni as a result of the electron transfer from Co to Ni, which is suggested by the XPS measurements. The absorbance of both linear- and bent-type NO bands are increased by alloying Co with Ni, as shown in Fig. 4. These increased absorbances of linear- and bent-type NO suggest the creation of adsorption sites with new electron density as a result of electronic interaction between Co and Ni.

Effect of the Alloying on the Adsorption State of CO and H_2

Temperature-programmed desorption is powerful in determining the adsorption state of H_2 and CO (*33*). Since the XPS and infrared study showed that electronic interaction between Co and Ni greatly affected the adsorption property of the catalyst, it is expected that significant effects of alloying Co with Ni on CO hydrogenation might result from the changes in the adsorption behavior. Effects of alloying on the adsorption state of CO and H_2 were studied by TPD measurements (Fig. 5). The adsorption state of CO and H_2 were changed remarkably by alloying. A rather high temperature is re-

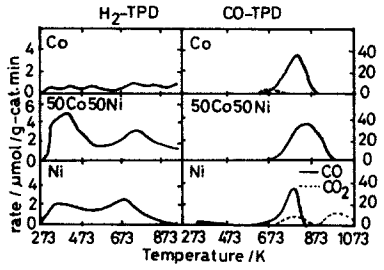

FIG. 5. Desorption curves of hydrogen and carbon monoxide from Co, Ni, and 50Co50Ni alloy.

quired for reducing Co compared with Ni. However, XPS and XRD analyses suggest that not only cobalt oxide but also nickel oxide did not exist in the alloy catalysts. Therefore, effects of the degree of reduction could be neglected in this study. Alloying Co and Ni enhances the adsorption amount of H_2 and CO. In particular, the desorption amount of H_2 below 573 K was greatly increased. Comparing with carbon monoxide, an alloy effect was obviously observed on the adsorption state of hydrogen. The change in the adsorption state of CO and H_2 on alloy catalysts seems to result from the creation of the adsorption sites with new electron density, which are suggested by the infrared spectra of adsorbed NO and the XPS spectra. The desorption amount of CO was generally larger than that of H_2 by an order of magnitude. In addition, most of the preadsorbed CO on these catalysts desorbed in a higher temperature region compared with the preadsorbed H_2. Chemisorption of carbon monoxide seems to be much stronger than that of hydrogen on the alloy catalysts. The surface concentration of hydrogen and carbon monoxide plays a decisive role for determining the catalytic activity and the selectivity in CO hydrogenation.

The effect of alloying Co with Ni was investigated based on the Langmuir adsorption model as below (*14*),

$$H_2(g) + 2* \underset{k_d^H}{\overset{k_a^H}{\rightleftharpoons}} 2H(a) \qquad (2)$$

$$CO(g) + * \underset{k_d^{CO}}{\overset{k_a^{CO}}{\rightleftharpoons}} CO(a), \qquad (3)$$

where the asterisks (*) represent unoccupied surface sites, and the subscripts (g) and (a) indicate the gas phase and the adsorbed species, respectively. It is well known that the heats of chemisorption of hydrogen and CO decrease as the coverage increase. However, these influences are neglected in this study for simplification. The surface concentrations of H_2 and CO calculated by the Langmuir model reflect the actual ones reasonably well according to Raupp and Dumesic (*13, 14*). The equilibrium surface concentration coverage of H and CO was obtained as the following equations by assuming that hydrogen adsorbs dissociatively and that catalytic reaction between adsorbed H and CO species is absent (*14*),

$$\theta_H = \frac{(k_a^H P_{H_2}/k_d^H)^{1/2}}{1 + (k_a^H P_{H_2}/k_d^H)^{1/2} + (k_a^{CO} P_{CO}/k_d^{CO})} \qquad (4)$$

$$\theta_{CO} = \frac{k_a^{CO} P_{CO}/k_d^{CO}}{1 + (k_a^H P_{H_2}/k_d^H)^{1/2} + (k_a^{CO} P_{CO}/k_d^{CO})}, \qquad (5)$$

where P_{H_2} and P_{CO} are the partial pressure of H_2 and CO, respectively. The following expression gives the desorption rate (r_d) without readsorption (*32*),

$$r_d = k_d A \exp(-E_d/RT), \qquad (6)$$

where A stands for the adsorbed amount, and E_d is the activation energy for desorption. The activation energy, E_d was obtained from the slope of the straight lines between $\ln(r_d/A)$ and T^{-1}, and thus the desorption rate constant (k_d) at 523 K can be estimated from Eq. (6) by using the thus-obtained E_d and the measured r_d. Desorption rate constants for CO and H_2 were enhanced by alloying Co with Ni, as is summarized in Table 1. On the other hand, the adsorption rates of CO and H_2 were expressed as the following equations:

$$r_a^H = k_a^H P_{H_2}(1 - \theta_H)^2 \qquad (7)$$

$$r_a^{CO} = k_a^{CO} P_{CO}(1 - \theta_{CO}). \qquad (8)$$

Since the surface coverage of hydrogen and carbon monoxide can be approximated to be 0 in the initial stage of adsorption, the adsorption rate of CO and H_2 was simply expressed as

$$r_a^H = k_a^H P_{H_2} \qquad (9)$$

$$r_a^{CO} = k_a^{CO} P_{CO}. \qquad (10)$$

TABLE 1

Adsorption Rate Constant, Desorption Rate Constant, and Surface Coverage of H_2 and CO on Co, Ni, and 50Co50Ni Alloy Catalysts

Catalyst	CO adsorption (min^{-1})		H_2 adsorption (min^{-1})		Surface coverage	
	k_a^{CO}	k_d^{CO}	k_a^H	k_d^H	θ_{CO}	θ_H
Co	0.257	0.090	0.729	0.021	0.984	0.016
50Co50Ni	0.225	0.228	0.934	0.029	0.956	0.044
Ni	1.901	0.157	2.324	0.013	0.986	0.014

Note. k_a^H, k_a^{CO}: adsorption rate constant of H_2 and CO at 523 K, respectively; k_d^H, k_d^{CO}: desorption rate constant of H_2 and CO at 523 K, respectively; θ_{CO}, θ_H: calculation under 523 K, P_{H_2} = 64 kPa, P_{CO} = 32 kPa.

Time dependence of the adsorption amount of H_2 and CO at 523 K on 50Co50Ni/SiO_2 is shown in Fig. 6 as an example. Equations (9) and (10) could be applied within 40 sec after the introduction of CO and H_2, and the initial adsorption rate was estimated from the time-dependence of the adsorbed amount in this period. The adsorption rate constants are approximately estimated from the adsorption rate under the different partial pressure of hydrogen and carbon monoxide as shown in Fig. 7. The adsorption rate constants for CO and H_2 on Ni, Co, and 50Co50Ni are summarized in Table 1. By calculating with thus-obtained adsorption and desorption rate constants for CO and H_2, the surface coverage was estimated from Eqs. (4) and (5) under the hydrogenation condition of CO, i.e., 523 K, p_{CO} = 320 kPa, P_{H_2} = 640 kPa (Table 1). The nickel and cobalt surfaces are nearly saturated with carbon monoxide in the absence of catalytic reaction. Alloying Co with Ni alters the adsorption strength of CO and H_2 as shown in Fig. 4, and leads to a higher hydrogen surface coverage. Raupp and Dumesic (*13, 14*) reported that the catalytic activity for methanation on Ni catalyst primarily depends on the extent of inhibition to hydrogen adsorption by adsorbed CO. The low hydrogenation activity for carbon monoxide on Co/SiO_2 or Ni/SiO_2 seems to result from the extremely low surface coverage of hydrogen. Alloying Co with Ni increases the H-adatom coverages on metal under steady-

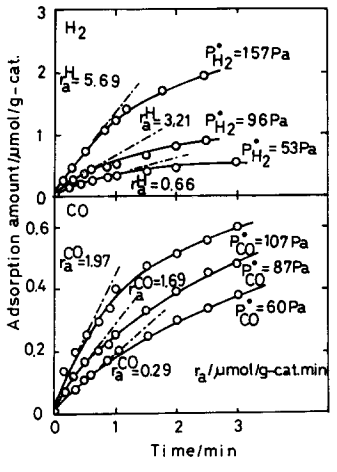

FIG. 6. Time dependence of the adsorption amount of H_2 and CO on 50Co50Ni/SiO_2 catalyst under various initial pressures. Adsorption temperature; 523 K.

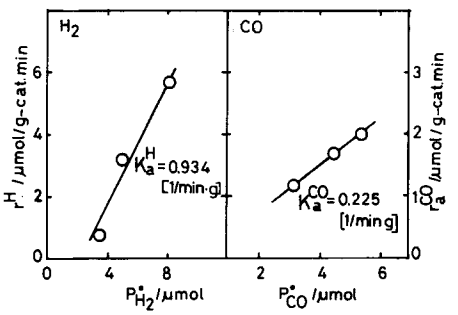

FIG. 7. Plots of the adsorption rate against the initial partial pressure of H_2 and CO.

TABLE 2

Rate of H_2–D_2 Exchange Reaction over Supported Co–Ni Alloy Catalysts

Catalyst	Before CO adsorption			After CO adsorption		
	Exchange rate (mol/min)		E_a (kcal/mol)	Exchange rate (mol/min)		E_a (kcal/mol)
	195 K	273 K		273 K	298 K	
Co	8.28×10^{-6}	1.37×10^{-4}	3.8	1.34×10^{-6}	4.87×10^{-6}	7.8
75Co25Ni	3.74×10^{-5}	3.39×10^{-4}	3.0	2.32×10^{-5}	9.10×10^{-5}	8.8
50Co50Ni	3.89×10^{-4}	1.63×10^{-3}	1.7	1.69×10^{-5}	8.45×10^{-5}	10.4
25Co75Ni	5.66×10^{-4}	1.67×10^{-3}	1.4	2.32×10^{-5}	9.10×10^{-5}	8.8
Ni	8.25×10^{-4}	1.60×10^{-3}	0.9	6.47×10^{-5}	8.65×10^{-5}	1.9

state conditions of CO hydrogenation, and should lead subsequently to the higher reaction rate of hydrogen. It appears that the new adsorption sites created by allowing Co with Ni have a distinct electron density from those of Co and Ni single metal. On the adsorption sites with the distinct electron density, the adsorption of CO should be weakened, and thus the amount of surface hydrogen is enlarged by alloying compared with those on Co and Ni. Increased surface coverage of hydrogen, therefore, seems to result from these new adsorption sites created by alloying Co with Ni.

Effect of Alloying on the Dissociative Adsorption of Hydrogen

Hydrogen-isotope exchange reaction is a useful model reaction for estimating the reactivity of hydrogen on catalysts (*34*). The rates of H_2–D_2 exchange on SiO_2-supported Co–Ni alloy catalyst before and after CO adsorption are summarized in Table 2. Since the exchange rate was very low and the activation energy was high on Co/SiO_2, the reactivity of adsorbed hydrogen on Co/SiO_2 seems to be low. On the contrary, Ni/SiO_2 catalyst exhibited an extremely high exchange rate and a low activation energy. This suggests that Ni/SiO_2 catalyst is active for the hydrogen activation. Both the rate for H_2–D_2 exchange and the activation energy on Co–Ni alloy catalyst are intermediate between Co and Ni. No relationship, however, has been found between the CO hydrogenation activity and the H_2–D_2 exchange rate without carbon monoxide. This suggests that the catalytic activity of alloy for hydrogenation altered radically with the presence of CO because of the low hydrogen concentration on the metal surface as suggested by the Langmuir adsorption model.

Preadsorbed carbon monoxide greatly reduced the overall rate of H_2–D_2 exchange. Since the exchange rate was restored to the value before CO adsorption by an evacuation at 673 K, the dissociative adsorption of hydrogen was strongly impeded by the CO adsorption. The overall rate of CO hydrogenation is plotted versus the rate of H_2–D_2 exchange reaction after CO adsorption, which reflects the activity of catalyst for the dissociative adsorption of hydrogen in the presence of CO. The rate of H_2–D_2 exchange reaction is obtained by the extrapolation of Arrhenius plots for H_2–D_2 exchange reaction to 523 K over CO-preadsorbed Co–Ni alloy (Fig. 8). The CO hydrogenation rate evidently correlated with the H_2–D_2 exchange rate in the presence of CO. As a result, the activation of H_2 under the presence of CO is of primary importance in determining the CO hydrogenation rate in these Co–Ni alloy catalysts. The chemisorption of CO is so strong on Co and Ni that very few adsorption sites are available for hydrogen adsorption. The low CO hydrogenation activity on Co/SiO_2 and Ni/

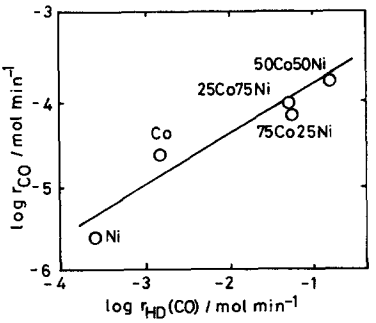

FIG. 8. Relation between the CO hydrogenation rate and the rate of H_2–D_2 exchange reaction on the CO preadsorbed Co–Ni alloy catalyst.

SiO_2, therefore, results from the low activity for the dissociative adsorption of hydrogen in the presence of CO. However, the alloying Co with Ni gives rise to adsorption sites with a new electron density as a result of the electronic interaction between Co and Ni in the outer shell orbital. Since the adsorption of CO seems to be weakened on these adsorption sites created by alloying Co with Ni, a higher hydrogen coverage in the presence of CO can be attained on the Co–Ni alloy catalyst. Alloying Co with Ni, therefore, leads to a high activity for hydrogen dissociative adsorption resulting in the high catalytic activity for CO hydrogenation. The chain growth probability was also elevated by alloying Co with Ni. This is because both hydrogen and carbon monoxide are easily chemisorbed to form the intermediate of partially hydrogenated species on the catalyst surfaces. As a result, alloying Co with Ni is effective for enhancing the gasoline yield.

CONCLUSIONS

Alloying Co with Ni exhibited a marked effect on the catalytic activity in CO hydrogenation. In particular, 50Co50Ni exhibited extremely high CO conversion, six times higher than that of Co and Ni. XPS spectra for the $3p_{3/2}$ orbital of Co and Ni and infrared spectra of adsorbed NO confirmed that there is some electron donation from Co to Ni in Co–Ni alloy. Model calculation for surface coverage by hydrogen and carbon monoxide shows that alloying Co with Ni leads to a high H-adatom surface concentration. Moreover, the exchange reaction of H_2–D_2 on CO-preadsorbed catalysts suggests that the dissociative adsorption of hydrogen is of primary importance in determining the catalytic activity of this alloy system, since the surface CO species strongly hinder hydrogen adsorption. Alloying Co with Ni, therefore, weakens the CO adsorption and allows hydrogen to chemisorb more easily on the metal surface. The alloy effect in the present study seems to result from the control of surface concentrations of active hydrogen by the electronic interaction in the outer shell orbital of Co and Ni.

REFERENCES

1. Burch, R., *Acc. Chem. Res.* **1982,** 24 (1982).
2. Ott, G. L., and Fleisch, T., and Delgass, W. N., *J. Catal.* **65,** 253 (1980).
3. Jiang, X. Z., Stevenson, S. T., and Dumesic, J. A., *J. Catal.* **91,** 11 (1985).
4. Amelse, J. A., Schwartz, L. H., and Butt, J. B., *J. Catal.* **87,** 179 (1984).
5. Lin, T. A., Schwartz, L. H., and Butt, J. B., *J. Catal.* **97,** 177 (1986).
6. Ishihara, T., Eguchi, K., and Arai, H., *Appl. Catal.* **30,** 225 (1987).
7. Ishihara, T., Eguchi, K., and Arai, H., *Appl. Catal.* **40,** 87 (1988).
8. Horiuchi, N., Ishihara, T., Eguchi, K., and Arai, H., *Chem. Lett.* **1988,** 499 (1988).
9. Paál, Z. and Menon, P. G., *Catal. Rev.-Sci. Eng.* **25,** 229 (1983).
10. Reoethlein, R. J., *J. Electrochem. Soc.* **116,** 37 (1969).
11. Breitev, M. W., *Electrochim. Acta.* **29,** 711 (1984).
12. Vannice, M. A., Hasselbring, C. C., and Sen, B., *J. Phys.* **89,** 2972 (1985).
13. Raupp, G. B., and Dumesic, J. A., *J. Catal.* **95,** 587 (1985).
14. Raupp, G. B., and Dumesic, J. A., *J. Catal.* **96,** 597 (1985).
15. Bartholomew, C. H., Parnell, R. B., Butler, J. L., and Mustard, D. G., *Ind. Eng. Chem. Prod. Res. Dev.* **20,** 296 (1981).
16. Arai, H., and Tominaga, H., *J. Catal.* **43,** 131 (1976).
17. Yasumori, I., and Ohno, S., *Bull. Chem. Soc. Jpn.* **39,** 302 (1966).

18. Matsuyama, M., Ashida, K., and T. Kakeuchi, *J. Catal.* **102,** 309 (1986).
19. Rodriguez, J. A., Campbell, R. A., and Goodman, D. W., *J. Phys. Chem.* **95,** 5716 (1991).
20. Boccuzzi, F., Chiorino, A., Ghiotti, G., Dinna, F., Strukul, G., and Tessari, R., *J. Catal.* **126,** 381 (1990).
21. Primet, M., Mathieu, M. V., and Sachtler, W. M. H., *J. Catal.* **44,** 325 (1976).
22. Sinfelt, J. H., Carter, J. L., and Yates, D. J. C., *J. Catal.* **24,** 290 (1972).
23. Verbeek, B. H., *Solid State Commun.* **44,** 951 (1982).
24. Chen, M. I., Cheng, C. T., and Yeh, C. T., *J. Catal.* **95,** 346 (1985).
25. Hufner, S., Wertheim, G. K., Cohen, R. L., and Wernich, J. H., *Phys. Rev. Lett.* **28,** 488 (1972).
26. Hufner, S., Wertheim, G. K., and Wernich, J. H., *Phys. Rev. B* **8,** 4511 (1973).
27. Stocks, G. M., Wiliams, R. W., Faulkner, J. S., *Phys. Rev. B* **4,** 4390 (1971).
28. Kallne, E., *J. Phys. F: Metal Phys.* **4,** 164 (1974).
29. Wandelt, K., and Ertl, G., *J. Phys. F: Metal Phys.* **6,** 1607 (1976).
30. Houston, J. E., and Park, R. L., *J. Chem. Phys.* **55,** 4601 (1971).
31. Ishihara, T., Eguchi, K., and Arai, H., *Chem. Lett.* **1986,** 1695 (1986).
32. Michaelson, H. B., *J. Appl. Phys.* **48,** 4729 (1977).
33. Falconer, J. L., and Schwarz, J. A., *Catal. Rev.-Sci. Eng.* **25,** 141 (1983).
34. Ishihara, T., Horiuchi, N., Eguchi, K., and Arai, H., *J. Catal.* **130,** 202 (1991).